

Spin-orbit torque induced magnetization anisotropy modulation in Pt/(Co/Ni)₄/Co/IrMn heterostructure

Christian Engel, Sarjoosing Goolaup, Feilong Luo, Weiliang Gan, and Wen Siang Lew

Citation: *Journal of Applied Physics* **121**, 143902 (2017); doi: 10.1063/1.4980108

View online: <http://dx.doi.org/10.1063/1.4980108>

View Table of Contents: <http://aip.scitation.org/toc/jap/121/14>

Published by the *American Institute of Physics*



Small Conferences. BIG Ideas.

Applied Physics
Reviews

SAVE THE DATE!
3D Bioprinting: Physical and Chemical Processes
May 2–3, 2017 • Winston Salem, NC, USA

The background of the banner features a stylized, glowing blue and red network of lines, resembling a biological or chemical structure, set against a dark blue background with light rays.

Spin-orbit torque induced magnetization anisotropy modulation in Pt/(Co/Ni)₄/Co/IrMn heterostructure

Christian Engel, Sarjoosing Goolaup, Feilong Luo, Weiliang Gan, and Wen Siang Lew^{a)}
 School of Physical and Mathematical Sciences, Nanyang Technological University, 21 Nanyang Link,
 Singapore 637371

(Received 26 January 2017; accepted 1 April 2017; published online 14 April 2017)

In this work, we show that domain wall (DW) dynamics within a system provide an alternative platform to characterizing spin-orbit torque (SOT) effective fields. In perpendicularly magnetized wires with a Pt/(Co/Ni)₄/Co/IrMn stack structure, differential Kerr imaging shows that the magnetization switching process is via the nucleation of the embryo state followed by domain wall propagation. By probing the current induced DW motion in the presence of in-plane field, the SOT effective fields are obtained using the harmonic Hall voltage scheme. The effective anisotropy field of the structure decreases by 12% due to the SOT effective fields, as the in-plane current in the wire is increased. *Published by AIP Publishing.* [<http://dx.doi.org/10.1063/1.4980108>]

I. INTRODUCTION

Spin-Orbit coupling in structures comprising a heavy metal (HM) adjacent to a ferromagnetic material (FM) leads to an in-plane charge current inducing orthogonal pure spin current via bulk spin Hall effect (SHE) in the HM and an effective field via Rashba effect at the interface. The pure spin current transfers its spin angular momentum to the FM via the spin-orbit torque (SOT) which comprises Slonczewski-like and field-like torques.^{1–3} The SOT induced by the SHE has been proposed as an alternative writing mechanism in magnetic random access memory (MRAM) devices. The read and write paths can be decoupled in the proposed three-terminal magnetic tunnel junction (MTJ)⁴ while improving the reliability of the memory device.^{4,5}

To achieve deterministic SOT induced magnetization switching in FM systems with perpendicular magnetic anisotropy (PMA), an in-plane external magnetic field is required.⁶ To achieve a field-free SOT induced magnetization switching, various approaches have been proposed to create an intrinsic in-plane tilt of the FM spins. Different methods have been proposed; the utilization of an external in-plane field, a tilted magnetic FM layer leading to an unbalance of the out-of-plane anisotropy and the introduction of an antiferromagnetic layer (AFM) which produces a current dependent in-plane exchange bias field to the FM layer. The externally applied in-plane field breaks the symmetry switch the magnetization.^{2,4,7} Similarly, the tilted FM layer may produce through an inhomogeneous magnetic out-of-plane anisotropy an intrinsic effective in-plane field which helps in breaking the symmetry for magnetization switching.⁸ The use of an AFM with in-plane exchange bias has been shown to lead to deterministic magnetization switching.^{9–11}

In this work, we investigate the current induced effects in an out-of-plane exchange biased PMA structure comprising a Pt/[Co/Ni]₄/Co/IrMn₃ stack where both the Pt layer and IrMn layer are considered as a source of SOT effective

fields. By leveraging on the domain wall (DW) nucleated during the magnetization reversal process, the SOT effective fields can be determined using conventional harmonic Hall measurement. The current induced effects also lead to a modification of the out-of-plane anisotropy of the stack structure. A decrease of ~ 600 Oe in the anisotropy field is obtained as the current is increased from 3.7×10^{10} to 8.3×10^{10} A/m².

II. EXPERIMENTAL DETAILS

A HM/FM/AFM stack was grown by DC magnetron sputtering at room temperature on 300 nm thick SiO₂ on Si substrates. The stack structure comprises SiO₂/Ta(5)/Pt(5)/[Co(0.25)/Ni(0.5)]₄/Co(0.25)/IrMn₃(10)/Ta(5) where the numbers in brackets correspond to the respective film thicknesses in nm. No field or heat treatment has been carried out after deposition of the film. The out-of-plane magnetization (M-H) loop obtained using polar MOKE for the HM/FM/AFM stack is shown in Figure 1(a). The as-grown HM/FM/AFM film exhibits a clear out-of-plane magnetic anisotropy with a coercivity of 265 Oe and an out-of-plane exchange bias field of 145 Oe. The magnetization switching in the negative field occurs at much higher magnitude compared to the positive field. This can be explained by the exchange bias field from the AFM layer promoting magnetization alignment along the +z orientation.

The film is patterned into 4 μm wide and 70 μm long wire via electron beam lithography. Hall bar contacts comprising Ta/Cu/Au were patterned transverse to the wire orientation, along the y-axis, as shown in the inset in Fig. 1(b). Magnetotransport measurements were carried out in order to investigate the effect of the bias current on the magnetization of the HM/FM/IrMn stack.^{12,13} For this measurement, a Keithley 6221 AC source was used to apply the alternating current. To obtain a good signal-to-noise ratio in our experiment, all the measurements were conducted while flowing an AC bias current with a frequency of 309 Hz and the signals were measured using a 7265 Dual Phase DSP Lock-In

^{a)}Author to whom correspondence should be addressed. Electronic mail: wensiang@ntu.edu.sg

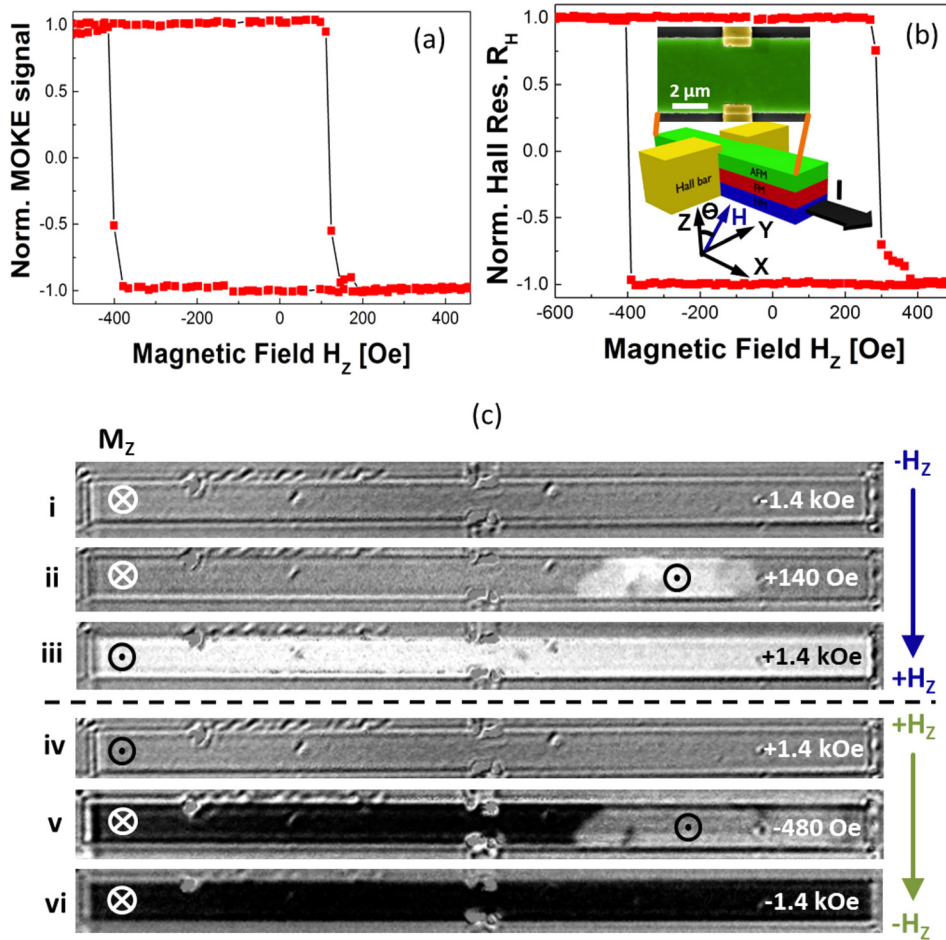


FIG. 1. (a) Normalized polar MOKE signal as a function of the applied field along the film normal of the bulk film comprising the stack Ta/Pt/[Co/Ni]₄/Co/IrMn/Ta. (b) Normalized Hall resistance as a function of applied field for a bias current of 1 mA in the patterned wire. The inset depicts a schematic and SEM image of our Hall bar structure. (c) Differential polar magneto-optic Kerr imaging microscopy images as a function of applied out-of-plane magnetic fields.

Amplifier. The low AC frequency allows for an adiabatic change of the magnetization vector. Magneto-Optical Kerr imaging was performed while sweeping an external field in the out-of-plane orientation.

III. RESULTS AND DISCUSSION

A. Effect of bias current on switching field

Coercivity and exchange bias field of the patterned wire as a function of externally applied fields and AC bias were first investigated. The Hall resistance (R_H) was measured via the anomalous Hall effect (AHE) by sweeping the applied magnetic field perpendicular to the plane of the wire, H_z . To obtain a sensible signal, a low AC channel current of 1 mA was applied in the wire. The Hall resistance R_H of the wire, as a function of applied magnetic field H_z , (R_H - H_z loops) for an AC channel current of 1 mA is shown in Fig. 1(b). From the AHE loop, the magnetization switching of the wire occurs at an external field of +300 Oe and -400 Oe, respectively. This implies that the coercivity of the patterned wire is 350 Oe, while the exchange bias field is estimated to be 50 Oe. As expected, the coercivity of the patterned wire exhibits an increase of ~ 85 Oe, as compared to the bulk film. The decrease in the exchange bias field is attributed to the patterning process.

In order to understand the magnetization reversal process in the wire, *in situ* differential Kerr microscopy was carried out while varying the externally applied field, H_z , as

shown in Figure 1(c). Reference Kerr images are first taken at positive and negative saturation field. The subsequent magnetic images are then obtained by subtracting the Kerr images from the reference image. As such, for no magnetization switching with respect to the reference, the corresponding differential Kerr image results in no magnetic contrast, corresponding to grey color in the Kerr image. At remanence, a grey contrast is observed, corresponding to the initial magnetization configuration being along the $+z$ or $-z$ orientation. For Figures 1(c-i)–1(c-iii), the wire was initially magnetized along $-z$ orientation by first applying an out-of-plane field of -1400 Oe. The reference Kerr image was taken at -1400 Oe as shown in Fig. 1(c-i). Subsequently, the externally applied field is ramped up along the $+z$ direction where an oppositely magnetized domain, characterized by the bright contrast in Fig. 1(c-ii), is nucleated in the wire, at an external field of 140 Oe. This is consistent with the switching field obtained from the R-H loop in Fig. 1(b) The reversed domain nucleates from the edge of the wire due to a reduction in the out-of-plane anisotropy at the edges of the wire from defects induced during patterning.¹⁴ Further increase in the external field leads to the expansion of the reversed domain, resulting in complete magnetization switching of the wire, Fig. 1(c-iii). For Figures 1(c-iv)–1(c-vi), the wire was initially magnetized along $+z$ orientation with an out-of-plane field of $+1400$ Oe and thereafter, the field was ramped along $-z$ direction. Using the state obtained at $+1400$ Oe, Fig. 1(c-iv) as a reference, grey contrast at no

magnetization reversal is imaged. As the externally applied field is increased in the $-z$ direction, the reversal process occurs via nucleation and propagation of the reversed domain in the wire, as seen by the dark contrast in Fig. 1(c-v). The expansion of the reversed domain results in complete magnetization switching. The Kerr image of Fig. 1(c-vi) corresponds to the complete magnetization reversal of the wire, resulting in a saturation state with a complete dark contrast. The Kerr imaging reveals that irrespective of the initial magnetization configuration, the switching process is via reversed domain nucleation and domain wall motion (DWM) along the wire.

To investigate the effect of current on the magnetization reversal process of the wire, the AC amplitude was varied from 1 to 12 mA, corresponding to current densities of 8.9×10^9 – 1.1×10^{11} A/m². An AC probing is chosen as it enables a better SNR due to the use of a lock-in system and also, it minimizes the Joule heating effect in the wire. The coercivity and exchange bias field are extracted from the AHE loops and are plotted as a function of the applied current as shown in Fig. 2. The coercivity decreases monotonically as the current is increased, from 350 to 120 Oe as the current magnitude is increased from 1 to 12 mA. On the other hand, the exchange bias field remains almost constant at ~ 55 Oe for all the current ranges investigated.

In all our Kerr imaging carried out, we noted that the reversal process is by the formation of an embryonic reverse domain state followed by the expansion of the reversed domain. The expansion of the reversed domain is via the propagation of a DW through the wire. It can be inferred that the measured coercivity in the AHE loop of Fig. 1(b) is correlated with the DWM along the wire axis, x direction. The coercive field obtained from the AHE measurement can then be viewed as being the field required to depin the DW at the Hall bar.

Current induced DW depinning field decrease has been reported for wires with both in-plane and out-of-plane magnetic anisotropy.^{15,16} The current leads to DW transformation via spin momentum transfer, resulting in a reduction of the depinning field.^{16,17} For the FM/HM stack, where the spin-orbit torque is dominant, the reduction in the depinning field has been attributed to the Slonczewski-like effective field from the SOT.¹⁸ For wires with FM/Cu stacks, no

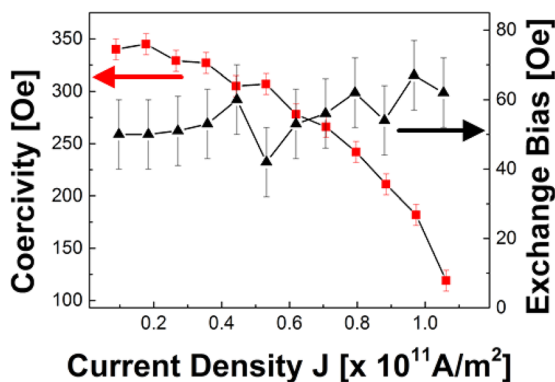


FIG. 2. Extracted coercivity and exchange bias fields from the Hall resistance hysteresis loop of the wire as a function of different AC.

change in depinning field was reported.¹⁸ In structures with out-of-plane magnetic anisotropy, the Slonczewski-like field can be read as $\mathbf{H}_{\text{SL}} \propto \mathbf{M} \times \mathbf{z} \times \mathbf{j}$ where \mathbf{j} is the unit vector in current direction, \mathbf{z} is the unit vector along the z -axis, and \mathbf{M} is the magnetization vector. The Slonczewski-like field acts along the current direction which is directed along the x -axis providing a torque transverse to the x -axis and the magnetization direction ($\boldsymbol{\tau} \propto \mathbf{H}_{\text{SL}} \times \mathbf{M}$).¹⁹ As the applied current is increased, the Slonczewski-like field increases proportionally, resulting in the DW internal spin aligning along the Slonczewski-like field orientation. The contribution of Joule heating on the reversal process can be neglected here, as the resistance change of the wire was negligible as the current was increased.

B. Probing of various DW types and current induced DW motion

To understand the current induced torques, the SOT effective fields in the system were characterized using the conventional Hall harmonic measurement technique.¹² In-plane magnetic field sweeps were performed in order to obtain the effective spin-orbit torque fields acting longitudinal (in x direction) or transverse (in y direction) to the long axis of the wire. In our stack, we expect the SOT effective fields to originate from both the Pt layer and the IrMn layer. The first harmonic Hall voltage, V_{ω} , for a PMA wire is given by¹³

$$V_{\omega} \approx \pm \frac{1}{2} \Delta R_{\text{AHE}} \left[1 - \frac{1}{2} \left(\frac{H \sin \theta_H}{H_K \pm H \cos \theta_H} \right)^2 \right] \Delta I, \quad (1)$$

where ΔR_{AHE} is the AHE resistance, H_K is the effective anisotropy field, H is the externally applied field, and θ_H is the external field angle with respect to the film plane normal (here, $\theta_H \approx 90^\circ$ for in-plane field sweeps). The \pm sign indicates the magnetization orientation along the $\pm z$ direction. For all measurements, an AC bias current was applied in the wire.

The representative Hall resistance (R_H) for an AC bias current of 5 mA, as the magnetic field was swept along the x -direction, is shown in Fig. 3(a). Two field sweeps were performed: positive field sweep where the magnetic field is swept from zero to maximum positive field, followed by a field sweep from maximum positive to maximum negative and then back to zero. For the negative field sweep, the magnetic field is swept from zero to maximum negative, then to maximum positive and finally to zero. For field sweep within the range of $+2000$ Oe to -2000 Oe, the Hall resistances display a parabolic trend for both magnetization orientations ($\pm z$) of the wire, as predicted by Equation (1).

For large external field sweeps, $|H| > 2000$ Oe, a sharp change in Hall resistance is observed at ± 2200 Oe as can be seen in Fig. 3(a). When the sample is magnetized along the $-z$ orientation, a sharp jump in Hall resistance is observed at $+2200$ Oe. Similarly, for the sample magnetized along the $+z$ orientation, a sharp drop in the Hall resistance value is noted at -2200 Oe. The increase/decrease in the Hall resistance at ± 2200 Oe results in almost similar Hall resistance

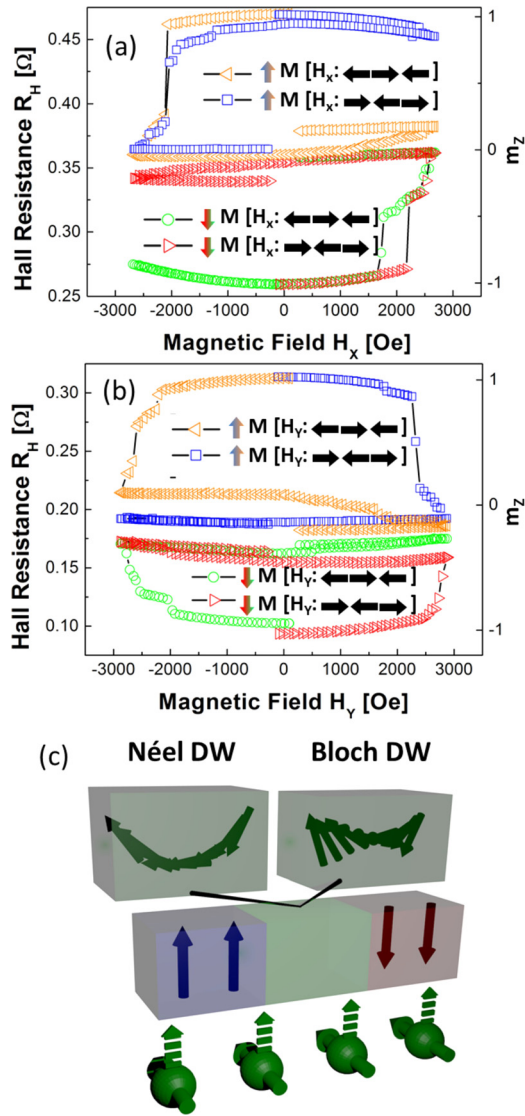


FIG. 3. Hall resistance as a function of externally applied fields. (a) Field swept along x direction, within a field range of ± 2800 Oe with an AC bias current of 5 mA. (b) Field swept in y direction, within the field range of ± 2800 Oe with an AC bias current of 10 mA. (c) Schematic configuration of Bloch and Néel domain wall types in a ferromagnetic structure. The Bloch wall is symmetric under a 180° rotation along the transverse axis to the wire whereas the Néel wall rotates along the wire axis. The bottom image depicts the contributions of spin current from the Pt underlayer.

magnitude, midway between the Hall resistance values obtained for $+z$ and $-z$ saturation magnetization, as seen in Fig. 3(a). This midway Hall resistance comprises the equal contributions in resistance from magnetization vectors aligned in the $+z$ and $-z$ orientation, corresponding to a half-switched state. Further field sweeps result in negligible change in the Hall resistance magnitude, implying that the half-switched state is a stable configuration at the Hall bar. The half-switched state is attributed to the presence of a pinned DW at the Hall cross. The Hall cross here acts as a potential barrier. The combination of current and external in-plane field induces magnetization reversal leading to the propagation of DW within the wire.

As the external field is applied along the x -axis, a chiral Néel DW configuration is favoured. The chirality of the Néel DW is determined by the initial orientation of the

magnetization and the DMI induced by the AFM layer^{20,21} or the interface between sublayer/FM layer. In our film stack comprising Pt/Co and interfaces, a left-handed chiral Néel DW is expected to be stabilized.²² The motion of a Néel DW in a wire is generally characterized by a surface tilting.²³ As such, the leading edge of the tilted Néel DW, on one side of the wire, encounters the pinning potential at the Hall cross first. Depending on the velocity of the DW, the DW can be pinned in the regions within the Hall cross. The depinning of the DW at the Hall cross might be due to a steady expansion and movement of the DW as the externally applied field is increased. This explains the steps in Hall resistance for different directions and the further change in Hall resistance after the sharp resistance drop/jump, which can be seen in Fig. 3(a).

For samples with initial magnetization along the $+z$ orientation, the Hall resistance change occurs for external fields applied along the $-x$ orientation as seen in Fig. 3(a). This implies that the DW propagates through the wire when the external magnetic field is applied along the $-x$ orientation. For external fields up to $+2800$ Oe, applied along the $+x$ orientation, no resistance drop, corresponding to no DW motion, was observed. This is consistent with the in-plane field induced DW propagation of a left-handed Néel DW with Up-Down configuration ($\uparrow \leftarrow \downarrow$). As shown in Fig. 3(c), Néel DWs gradually change their magnetization components along the wire long axis where the resulting Slonczewski-like field at the DW has an out-of-plane field component ($\mathbf{H}_{SL} \propto \mathbf{M} \times \mathbf{y}$).²⁴ Thus, the Slonczewski-like field is accountable for magnetization reversal in the structure as it produces an out-of-plane field component that drives the DW.

For field swept along y -axis, the same parabolic trend is expected for the first harmonic Hall voltage. Shown in Fig. 3(b) is the first harmonic Hall voltage measured with an AC bias current of 10 mA flowing through the wire. For field swept within -2200 Oe and $+2200$ Oe, the Hall resistance follows a parabolic trend as expected from Equation (1). Further increase in the magnetic field in the positive (negative) $-y$ direction leads to a sharp drop (jump) in the Hall resistance for samples magnetized in $+z$ ($-z$) orientation. Similarly to Fig. 3(a), the drop (jump) in the Hall resistance value results in a magnitude which is midway between the maximum and minimum Hall resistance values. Subsequent field sweeps do not influence the Hall resistance significantly. As discussed previously, a DW pinned at the Hall cross may account for the stable Hall resistance value. Interestingly, for the magnetic field swept transverse to the long axis of the wire, both the maximum positive and maximum negative field sweep result in a drop (jump) in Hall resistance. This implies that the DW within the wire can be driven by both orientations of applied fields, which was not observed in Fig. 3(a). The transverse applied field might transform the DW to a Bloch DW configuration within the wire. The transformation from a Néel to a Bloch DW will generally occur naturally as the magnetic vectors in the DW will prefer to align along the externally applied field. However, the DW driving field and depinning field for Bloch and Néel configurations are inherently different which, as a consequence, results in different depinning fields in our

measurement. This allows bidirectional motion of the DW as a function of the current and transverse field orientation.

For fields applied along the $+y$ -axis, transverse to the wire, the AC bias current was varied from 1 to 11 mA in the wire. The measured Hall resistance, for samples magnetized along the $+z$ orientation, is shown in Fig. 4(a). As the amplitude of the current was increased, the Hall resistance drop occurs at lower external fields. This drop in the Hall resistance corresponds to the pinning field of the DW at the Hall cross. The shift in the pinning field implies that the DW reaches the Hall cross at much lower external field as the current in the wire is increased. The dynamics of the DW is then governed by the external magnetic field and applied current induced SOT effective fields in the wire. As such, any shift in the DW pinning field is an indicator of the current induced torque on the DW dynamics in the wire. The pinning field corresponds to the external field where 50% of magnitude of the Hall resistance drop occurs. Using the DW pinning field at a bias current of 1 mA as reference, the difference in pinning field, ΔH_{pin} , as a function of different AC bias current, is computed. Shown in Fig. 4(b) is the pinning field difference as a function of the applied current. A quasi-linear trend is observed for high current magnitudes. The difference in external field ΔH_{pin} to pin the DW in the system for a current density of 8.3×10^{10} A/m², which translates to an effective current density of 7.4×10^{10} A/m² with respect to the reference at 0.9×10^{10} A/m², is calculated to be

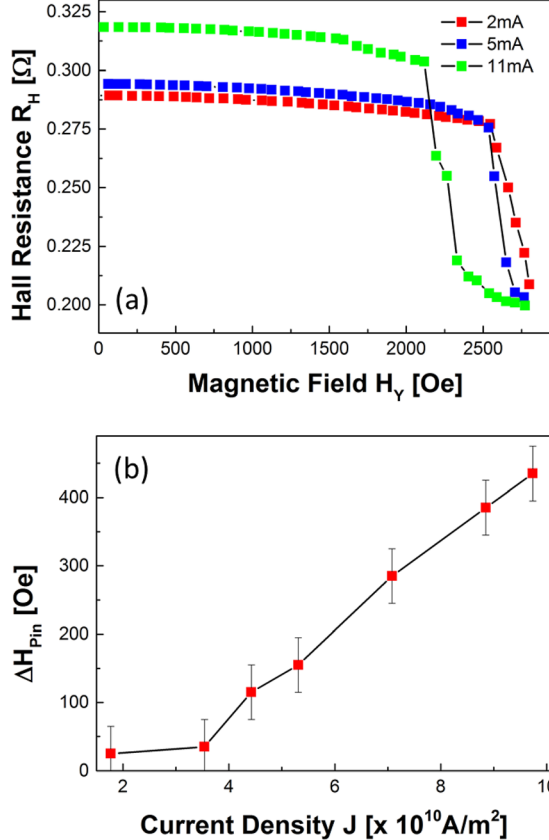


FIG. 4. (a) Hall resistance as a function of applied magnetic field transverse to the wire direction along y -axis for various currents in the wire. (b) The difference in transverse pinning field for a domain wall to the transverse pinning field at a current density of 8.9×10^9 A/m².

400 Oe \pm 50 Oe. We postulate that this difference in external field, ΔH_{pin} , can be attributed to the Field-like term of the SOT. The Field-like field aligns collinearly with the externally applied magnetic field which is swept transverse to the wire long axis in y direction. Any increase in the Field-like field due to current increase will be subtractive to the external field, as shown in Fig. 4(a). Consequently, the Field-like field can be extracted from first harmonic Hall voltage measurement by exploiting DW motion and pinning at the Hall cross. Using a similar approach as compared to field assisted DW depinning with SOT, where the depinning efficiency is given by $\Delta H_{pin}/\Delta J$,^{24,25} the depinning efficiency for SOT assisted DW depinning efficiency can be computed. From Figure 4, the SOT efficiency ($\Delta H_{pin}/\Delta J$) for the Field-like field is calculated to be ~ 63.7 Oe/(10^{10} A/m²).

C. Hall measurements to investigate effective SOT and anisotropy fields

To quantify the SOT effective fields, first (V_{ω}) and second ($V_{2\omega}$) harmonic Hall voltages were measured as a function of applied in-plane magnetic fields. The effective SOT fields can be extracted from the derivatives of the first and second harmonic Hall voltages¹

$$H_{SL,(FL)} \equiv -2 \left(\frac{\partial V_{2\omega}}{\partial H_{X,(Y)}} / \frac{\partial^2 V_{\omega}}{\partial H_{X,(Y)}^2} \right). \quad (2)$$

The Slonczewski-like field H_{SL} was extracted from the Hall voltage measurements while sweeping an external magnetic field along the x axes for various AC bias currents in the wire, as shown in Fig. 5(a). A linear trend in H_{SL} is observed, which is in agreement with previously reported results.^{1,26} For a current density of 8.3×10^{10} A/m², the effective Slonczewski-like field for magnetization aligned along $-z$ orientation is 61 Oe, whereas for magnetization oriented along the $+z$ direction, the effective field is 67 Oe. The difference between the effective Slonczewski-like field with up ($+z$) and down ($-z$) magnetization can be attributed to slight variation within the measurement setup. From Equation (1), we can also derive the effective anisotropy field H_K of the FM layer as a function of the current density in the wire. Using the fitting parameter to $b_{X,Y} = \partial^2 V_{\omega} / \partial H_{X,Y}^2$ and for externally applied in-plane fields, $\theta_H \approx 90^\circ$, the effective anisotropy field H_K can be computed as

$$H_K \approx \sqrt{\Delta I \Delta R_{AHE} / 2b_{X,Y}}. \quad (3)$$

The AHE resistance ΔR_{AHE} is calculated from Equation (1) as $\Delta R_{AHE} (= R_{H,max} - R_{H,min})$ to $0.220 \Omega \pm 0.003 \Omega$. The computed effective anisotropy field H_K from Equation (3) is plotted in Fig. 5(b).

The effective anisotropy field decreases linearly as a function of the applied current. As the current density is increased from 3.7×10^{10} to 8.3×10^{10} A/m², the anisotropy field reduces by ~ 600 Oe from 5700 Oe to 5100 Oe. Given that the effective anisotropy field is expressed as $H_K = 2K_{\perp} / M_S - 4\pi M_S$, we postulate that the current modulates the perpendicular anisotropy constant of the film stack. In general,

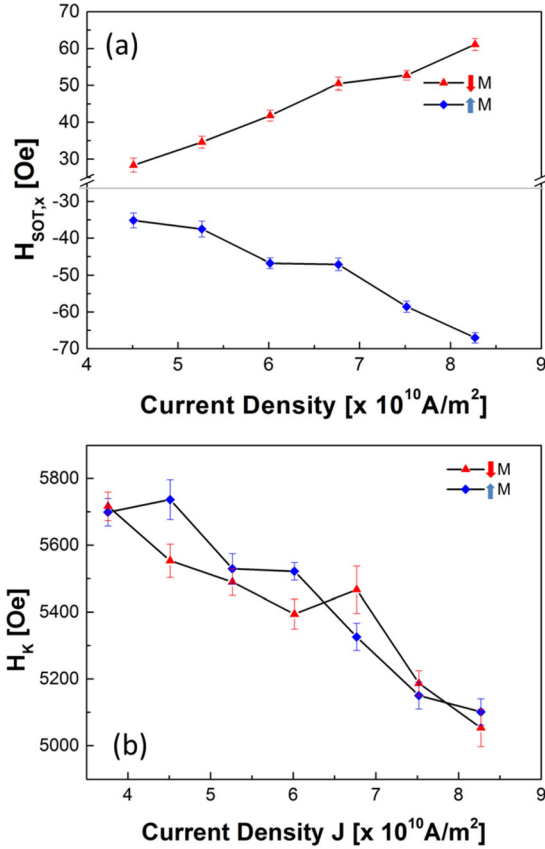


FIG. 5. (a) Slonczewski-like SOT field for $\pm z$ oriented magnetization (blue) and $-z$ oriented magnetization (red) as a function of the current density. (b) Effective anisotropy field computed from the first harmonic measurement with longitudinal field sweep as a function of the current density in the wire.

the magnetic anisotropy constant can be varied by the magnetic annealing effect, photoinduced magnetic anisotropy, crystallographic transformations, or roll magnetic anisotropy.¹⁷ In our experiment, the measurements were performed in a dark room at room temperature. As the Hall resistance was measured and taken into account for each current value and the SOT effective fields scale linearly with current, the temperature effect due to Joule heating can be neglected here. Therefore, this magnetic anisotropy decrease is due to spin-orbit torque effects.

Similar to the measurement conducted for the Slonczewski-field H_{SL} , the effective Field-like field H_{FL} is computed by measuring the first and second harmonic Hall voltages while sweeping the external magnetic field along the y -axis. In Figure 6, the effective Field-like field is shown as a function of the AC bias current density in the wire. As expected, the Field-like field increases linearly as a function of the applied current.^{1,22} For a current density of 8.3×10^{10} A/m², the Field-like field is computed to ~ 90 Oe for both orientations ($\pm z$) of magnetization. This value is 4 times smaller as compared to the measured effective Field-like field H_{FL} using DW pinning from Fig. 4(b). Harmonics measurement for quantifying the Field-like field term is known to give a lower value due to ignoring the contribution of the planar Hall effect (PHE) in the measurement. The measured Field-like field H_{FL} needs to be multiplied by a correcting factor which depends on the PHE to AHE

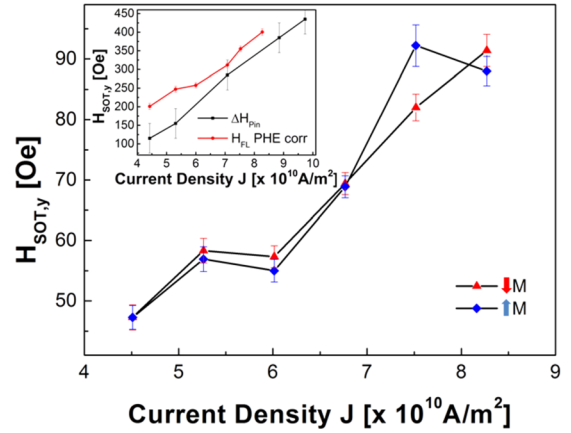


FIG. 6. Field-like SOT field for $\pm z$ oriented magnetization (blue) and $-z$ oriented magnetization (red) as a function of the current density in the wire.

ratio.^{13,25} The computation for the corrected Field-like field is obtained from Ref. 18 as

$$H_{FL,PHE corr} = \frac{H_{FL} + 2\zeta H_{SL}}{1 - 4\zeta^2}. \quad (4)$$

Assuming a PHE to AHE resistance ratio of 0.3 which is obtained from Ref. 24, the PHE corrected Field-like field H_{FL} using the harmonic measurement technique is computed to be ~ 400 Oe for a current density of 8.3×10^{10} A/m². This is in good agreement with our obtained result using DW motion as a detection method as can be seen in the inset of Fig. 6 where both computed fields are shown for $\pm z$ magnetization. The depinning field method using DWM is even underestimated which might indicate a lower PHE to AHE ratio or might be a result of the subtraction to a reference value in the field determination using DWM. Interestingly, the corrected Slonczewski-like effective field is found to be ~ 360 Oe for a current density of 8.3×10^{10} A/m², using the same PHE to AHE resistance ratio. This is in agreement with previous results.²⁷ From Equation (3), the anisotropy field H_K can be again extracted from the first harmonic Hall voltage obtained by sweeping field along the y -axis. For both magnetization orientation ($\pm z$), a decrease in the effective anisotropy field H_K is observed at similar values compared to the measurement while sweeping the field along the x -axis. This supports our measurement, where the effective magnetic anisotropy field is related to the AC bias current in the wire.

IV. CONCLUSION

DW dynamics in a Pt/(Co/Ni)₄/Co/IrMn stack structure with out-of-plane magnetic anisotropy and exchange bias has been investigated. Direct observation of magnetization switching via DW motion has been shown using the differential Kerr imaging microscopy technique. Field driven DW motion is shown to be an alternative mean to quantifying the SOT effective field in the system which is in good agreement with the harmonic Hall technique. Additionally, the bias current in the wire leads to a decrease in the effective magnetic anisotropy field, H_K , which can be attributed to SOT effective fields within the system.

ACKNOWLEDGMENTS

This work was supported by the Singapore National Research Foundation, Prime Minister's Office, under a Competitive Research Programme (Non-volatile Magnetic Logic and Memory Integrated Circuit Devices, NRF-CRP9-2011-01), and an Industry-IHL Partnership Program (NRF2015-IIP001-001). The work was also supported by a MOE-AcRF Tier 2 Grant (No. MOE 2013-T2-2-017). WSL is a member of the Singapore Spintronics Consortium (SG-SPIN).

- ¹J. Kim, J. Sinha, M. Hayashi, M. Yamanouchi, S. Fukami, T. Suzuki, S. Mitani, and H. Ohno, *Nat. Mater.* **12**, 240 (2013).
- ²L. Liu, O. J. Lee, T. J. Gudmundsen, D. C. Ralph, and R. A. Buhrman, *Phys. Rev. Lett.* **109**, 096602 (2012).
- ³C.-F. Pai, L. Liu, Y. Li, H. W. Tseng, D. C. Ralph, and R. A. Buhrman, *Appl. Phys. Lett.* **101**, 122404 (2012).
- ⁴L. Liu, C.-F. Pai, Y. Li, H. W. Tseng, D. C. Ralph, and R. A. Buhrman, *Science* **336**, 555 (2012).
- ⁵S. Ikeda, K. Miura, H. Yamamoto, K. Mizunuma, H. D. Gan, M. Endo, S. Kanai, J. Hayakawa, F. Matsukura, and H. Ohno, *Nat. Mater.* **9**, 721 (2010).
- ⁶P. P. J. Haazen, E. Murè, J. H. Franken, R. Lavrijsen, H. J. M. Swagten, and B. Koopmans, *Nat. Mater.* **12**, 299 (2013).
- ⁷I. M. Miron, *Nature* **476**, 189 (2011).
- ⁸G. Yu, P. Upadhyaya, Y. Fan, J. G. Alzate, W. Jiang, K. L. Wong, S. Takei, S. A. Bender, L.-T. Chang, Y. Jiang, M. Lang, J. Tang, Y. Wang, Y. Tserovnyak, P. K. Amiri, and K. L. Wang, *Nat. Nanotechnol.* **9**, 548 (2014).
- ⁹S. Fukami, C. Zhang, S. DuttaGupta, and H. Ohno, *Nat. Mater.* **15**, 535 (2016).
- ¹⁰W. J. Kong, Y. R. Ji, X. Zhang, H. Wu, Q. T. Zhang, Z. H. Yuan, C. H. Wan, X. F. Han, T. Yu, K. Fukuda, H. Naganuma, and M.-J. Tung, *Appl. Phys. Lett.* **109**, 132402 (2016).
- ¹¹Y.-C. Lau, D. Betto, K. Rode, J. M. D. Coey, and P. Stamenov, *Nat. Nanotechnol.* **11**, 758 (2016).
- ¹²U. H. Pi, K. W. Kim, J. Y. Bae, S. C. Lee, Y. J. Cho, K. S. Kim, and S. Seo, *Appl. Phys. Lett.* **97**, 162507 (2010).
- ¹³M. Hayashi, J. Kim, M. Yamanouchi, and H. Ohno, *Phys. Rev. B* **89**, 144425 (2014).
- ¹⁴D. Bhowmik, M. E. Nowakowski, L. You, O. Lee, D. Keating, M. Wong, J. Bokor, and S. Salahuddin, *Sci. Rep.* **5**, 11823 (2015).
- ¹⁵M. Hayashi, L. Thomas, C. Rettner, R. Moriya, X. Jiang, and S. S. P. Parkin, *Phys. Rev. Lett.* **97**, 207205 (2006).
- ¹⁶D. Ravelosona, D. Lacour, J. A. Katine, B. D. Terris, and C. Chappert, *Phys. Rev. Lett.* **95**, 117203 (2005).
- ¹⁷S. Chikazumi, *Physics of Ferromagnetism* (Oxford University Press, 1997), p. 488.
- ¹⁸K. K. Meng, J. Miao, X. G. Xu, J. X. Xiao, J. H. Zhao, and Y. Jiang, *Phys. Rev. B* **93**, 060406(R) (2016).
- ¹⁹A. Manchon and S. Zhang, *Phys. Rev. B* **78**, 212405 (2008).
- ²⁰R. Yanes, J. Jackson, L. Udvardi, L. Szunyogh, and U. Nowak, *Phys. Rev. Lett.* **111**, 217202 (2013).
- ²¹A. Thiaville, S. Rohart, É. Jué, V. Cros, and A. Fert, *Europhys. Lett.* **100**, 57002 (2012).
- ²²G. Chen, T. Ma, A. T. N'Diaye, H. Kwon, C. Won, Y. Wu, and A. K. Schmid, *Nat. Commun.* **4**, 2671 (2013).
- ²³E. Martinez, S. Emori, N. Perez, L. Torres, and G. S. D. Beach, *J. Appl. Phys.* **115**, 213909 (2014).
- ²⁴S. Emori, U. Bauer, S.-M. Ahn, E. Martinez, and G. S. D. Beach, *Nat. Mater.* **12**, 611 (2013).
- ²⁵O. Boulle, J. Kimling, P. Warnicke, M. Klauui, U. Ruediger, G. Malinowski, H. J. M. Swagten, B. Koopmans, C. Ulysse, and G. Faini, *Phys. Rev. Lett.* **101**, 216601 (2008).
- ²⁶S. Woo, M. Mann, A. J. Tan, L. Caretta, and G. S. D. Beach, *Appl. Phys. Lett.* **105**, 212404 (2014).
- ²⁷K. K. Meng, J. Miao, X. G. Xu, Y. Wu, X. P. Zhao, J. H. Zhao, and Y. Jiang, *Phys. Rev. B* **94**, 214413 (2016).